Multiple Excited States in a Two-State Crossing Model: Predicting Barrier Height Evolution for H + Alkene Addition Reactions

James S. Clarke,† Heather A. Rypkema, Jesse H. Kroll, Neil M. Donahue,* and James G. Anderson

Department of Chemistry and Chemical Biology, Harvard University, Cambridge, Massachusetts 02138

Received: August 26, 1999; In Final Form: February 25, 2000

In order to identify the underlying factors determining barrier heights when hydrogen atoms add to alkenes, we present a theoretical framework isolating the fundamental quantum-chemical properties involved and enabling evaluation of the relative influence of each property. This approach describes the control of these barriers and motivates a series of experimental measurements as a rigorous test. A two-state avoided curve crossing model provides the essential description, but only when multiple excited states are combined to yield a mixed state of dual covalent−ionic character. We show that variations in mixed-state energy drive the evolution in barrier heights, and that by selecting a set of test reactions with diverse energetic and overlap interactions, one may discover which of several excited states dominates this evolution. Results from the experimental test show conclusively that it is variation in the lowest ionic-state energy, and not variations in either singlet−triplet splitting or reaction enthalpy that drive barrier height evolution over the series of H + alkene addition reactions. Combining this result with our earlier results for H-atom abstraction reactions, we have demonstrated that barrier heights of essentially all radical−molecule reactions with electrophilic radicals are controlled by the excited ionic states formed by the transfer of an electron from the molecule to the radical.

Introduction

A fundamental understanding of chemical reactivity that translates into both a predictive accuracy of barrier heights and a context for thinking about the mechanisms controlling reaction probability remains a central objective of chemistry. For example, radical−molecule addition reactions constitute the rate-limiting steps in a wide range of important chemical systems. In the synthesis of organic compounds they provide a route for the formation of carbon−carbon bonds,[1,2] while in the atmosphere they initiate reaction sequences that produce ozone in the urban troposphere.[3] The room-temperature rate constants of these systems span more than 8 orders of magnitude, from the nearly gas-kinetic addition of the hydroxyl radical to isoprene,[4] to the extremely slow addition of ozone to ethene,[5] and beyond to the almost immeasurably slow rates for the gas-phase addition of ozone to haloalkenes. These addition reactions have barriers resulting from the conversion of the reactant wave function to the product wave function. In order to understand the enormous evolution in reactivity across these systems, the barriers to these reactions have been addressed as two-state curve crossings,[6−8] where the ground state and a single promoted state of the reactants map into the promoted and ground states of the products over the course of the reaction. Such a description allows properties of the separated reactants and products (ionization potential, electron affinity, singlet−triplet splitting, polarizability, etc.) to provide direct insight into the nature of the transition state. Analysis using a two-state crossing model has provided a comprehensive description of radical−molecule abstraction reactions,[8,9] where the barrier is largely a result of a crossing between the ground and ionic states of the reactants and products. However, there is ample evidence that the two-state description is a considerable oversimplification for radical-addition reactions.[7,10,11]

The two-state crossing model is an invaluable tool for studying and understanding radical−molecule reactivity. It is conceptually simple. Basic physics governs the progression of the reaction in the far field, allowing for the determination of boundary conditions for a linear curve crossing. Within this approach, the underlying control of barrier height can be understood; multiple observed properties of separated reactants and products exert a quantifiable influence on the barrier height. This is in stark contrast to both simple correlative methods and high-level quantum-mechanical calculations. Correlative plots of measured barrier height versus properties of the individual reactants or products (i.e., ionization potential or singlet−triplet splitting) or of the reaction (i.e., enthalpy) may give fortuitous results due to covariance among properties, and therefore give little insight into which properties dominate barrier evolution. Furthermore, such methods do not allow multiple properties to be tested in conjunction with each other. High-level ab initio calculations, on the other hand, remain practical for only the smallest of chemical systems,[12,13] and ultimately obscure the underlying physics of the reaction.

Success of the two-state model relies on the appropriate choice of the promoted state, which mixes with the ground state to form the transition state. This promoted state is assumed to be the excited state of the reactants that most strongly couples to the product ground state. There are several possible choices for the excited state. The first state is formed by the antibonding state of the bond being broken in the course of the reaction. This state is covalent; it is usually the triplet excited state of the molecule in the reaction, whose energy is related to the bond

* Corresponding author.
† Present address: Laboratorium für Organische Chemie, ETH Zürich, Universitätstrasse 16, CH-8092 Zürich, Switzerland.

10.1021/jp993051v CCC: $19.00
Published on Web 04/14/2000

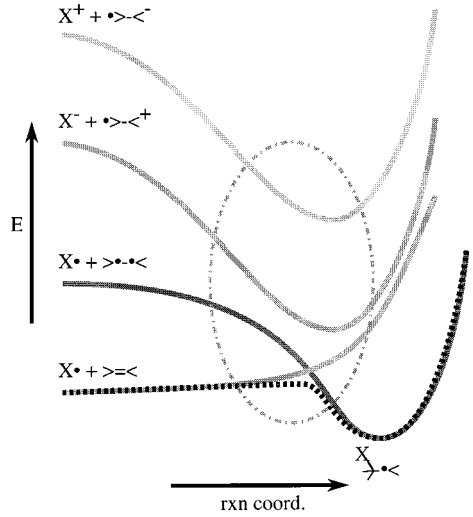

Figure 1. Reaction coordinate for the X + alkene addition reaction. The adiabatic surface (dotted line) is shown. In addition, the ground and three excited states of the reactants are shown. These are the excited state formed by the singlet−triplet excitation of the alkene, the excited state formed by transferring an electron from the alkene to X, and the excited state formed by transferring an electron from X to the alkene. The latter two excited states are ionic. Near the transition state (gray oval), these excited states strongly mix with the ground state to produce the adiabatic surface.

dissociation energy of the breaking bond.[14] The second type of excited state is formed by the transfer of an electron from the frontier molecular orbital (FMO) of one species to the FMO of the other. These are usually the highest occupied (HOMO) or lowest unoccupied (LUMO) molecular orbital of the molecule and the singly occupied orbital (SOMO) of the radical. This state is ionic.

Some reactions are controlled exclusively by ionic excited states (i.e., H-atom abstraction by electrophilic radicals[8]), while others are controlled exclusively by covalent excited states (i.e., alkyl radical additions to alkenes[10]). Each of these regimes is easily described with an appropriately formulated two-state curve crossing model. Yet, what controls the transition between the two regimes? When covalent and ionic excited-state energies are similar, which states contribute most strongly to the transition-state energy of a given reaction? Which states influence the variation in the transition-state energy from reaction to reaction in a homologous series? Finally, can we still pose a two-state crossing model in this mixed regime?

Hydrogen atom additions to alkenes and haloalkenes are an ideal test system for these questions. The covalent and ionic states are competitive, reactivity varies widely, and associated molecular properties (i.e., ionization potential, singlet−triplet splitting, and π-electron density) are correspondingly variable. Three distinct excited states may contribute significantly. These are (1) the state formed by the antibonding triplet of the alkene, (2) the state formed by transferring an electron from the alkene to the radical, and (3) the state formed by transferring an electron from the radical to the alkene. These three states are illustrated in Figure 1 for the generalized reaction coordinate of a radical-addition reaction. Near the transition state, each of these excited states configurationally mixes with the ground state to produce an adiabatic reaction surface. The relative contribution of each of these states is determined by the mixing, or delocalization, of the excited state with the ground state. If more than one of these states is significant in determining the adiabatic reaction surface, then the two-state model is an oversimplification. Our goal is first to develop a method by which we can accommodate this complication while still exploiting the simplicity of the two-state model, and second to use the resulting model to test data in order to quantitatively assess the role of these various states in controlling barrier height. To do this, we must extend our existing theory and measure a series of H-atom addition rate constants with the wide range of reactivity described above.

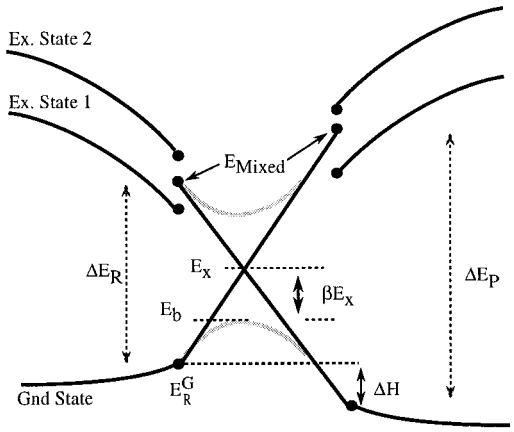

Figure 2. Graphical representation of the two-state crossing model. The energy gaps ΔE_R, ΔE_P, and ΔH are shown. These establish the crossing height, E_X, as given by eq 1. Strong quantum-mechanical mixing of these states lowers the energy of the adiabatic surface to give the barrier height, E_b. In a reaction where multiple excited states control reactivity, the two-state model can be useful if a mixed excited state, E_{Mixed}, is described and used as a boundary condition.

Theoretical Approach

In this section, we briefly discuss the two-state crossing model, the nature of the possible excited states, and the degree of interaction of each state with the ground state, as applicable to radical−molecule addition reactions. These topics are discussed in much greater detail in two previous papers.[8,9] In addition, we discuss the construction of a mixed excited state in order to incorporate multiple excited states into the two-state model.

Two-State Curve Crossing. For atom abstractions, we separate the reaction into three stages: undistorted approach, atom transfer (distortion), and undistorted withdrawal. We use different approximations to understand the energetic evolution of the excited states in each stage. In the case of radical-addition reactions, the reaction is not symmetric, and we separate the reaction into only two stages: undistorted approach and distortion culminating in the stable addition product. During the first stage of the reaction, the energies of the ground and excited states develop in the far field due to long-range attractive or repulsive forces. During the second stage of the reaction, where configurational mixing dominates and energy evolves due to the rehybridization of the reacting carbon in the molecule ($sp^2 \rightarrow sp^3$), we assume a linear, avoided curve crossing.

The energies of the unperturbed ground state and the excited state at the end of the approach stage serve as boundary conditions for the linear curve crossing (see Figure 2). The approach stage may be halted at any interaction distance, and a curve crossing height calculated. At some distance, this crossing height will be minimal. This distance corresponds to the transition state.

The curve-crossing height, E_X, at the transition state is given by

$$E_X = E_R^G + \frac{\Delta E_R(\Delta E_P + \Delta H)}{\Delta E_R + \Delta E_P} \qquad (1)$$

where E_R^G is the ground-state energy of the reactants at the end of the approach stage, ΔE_R is the energy gap between the ground and excited state of the reactants, ΔE_P is the energy gap of the products, and ΔH is the reaction enthalpy. Near the crossing, however, the wave functions for the ground and excited states strongly mix, reducing the energy of the system from the crossing point and producing the adiabatic reaction barrier. The energy of this barrier is some fraction of the crossing height and is given by

$$E_b = E_X(1 - \beta) \tag{2}$$

where β represents the coupling between the excited states. For reactions such as those studied here, the coupling is large; the actual barrier to reaction is much smaller than the crossing energy.

Our primary focus is on the evolution of this barrier height over a series of reactions ($dE_b/d(rxn)$). In this context, any errors associated with the linear curve crossing assumption are second order; heuristically, the effect of a nonlinear diabatic curve shape can be expressed by a multiplicative term, $F(\rho)$, where ρ is the reaction coordinate in the curve crossing region. This term is determined by the shape of the overlapping molecular orbitals producing a functional evolution of molecular overlap between the reactants, $ds/d\rho$. The derivative term $dF/d(rxn)$ will be small for a homologous series of reactions. This concept is well developed in the literature[14] and in our earlier treatments of this topic.[8,9]

The curve crossing height as given by eq 1 depends on four distinct boundary conditions. The first boundary condition is the energy of the reactant ground state, E_R^G, which anchors the curve crossing. The product ground state, which is incorporated into the curve crossing problem through the enthalpy of reaction, ΔH, sets the second boundary condition. The reactant ground state can develop in the far field due to long-range dipole−dipole and dipole−induced dipole interactions. These interactions lead to pre-reactive complexes, which can significantly perturb the potential energy surface and greatly influence the curve crossing height. At the extreme, the binding energy of this complex can be greater than the crossing height, producing a transition state with lower energy than the reactants. While the progression of the ground-state energies can be successfully modeled,[9] careful selection of the reactants allows this energy to be systematically varied. In this work we will effectively eliminate it by choosing a series of reactions where the ground-state energy does not vary from reaction to reaction.

The remaining two boundary conditions are determined by the heights of the reactant and product excited states. As illustrated in Figure 1, there are three low-lying excited states of both the reactants and products: one covalent state and two ionic states. Thus, a boundary condition is not well constrained by the energy of any one excited state. Yet the two-state model remains valid if a mixed excited state can be determined from the component states. For the products, the participating excited states are heavily mixed and are not easily modeled. However, these energies may be constrained by experimental studies on the excited states of the stable adduct. In order to determine the appropriate boundary condition for the reactant excited states, the energies and overlaps of both the covalent state and the ionic states with the ground state must be understood. These are discussed below.

Covalent Excited States. The covalent excited states are formed from the vertical singlet → triplet excitation in the π bond of the alkenes. Along the reaction coordinate, the electron promoted to the antibonding orbital of the π bond maps into the bond being formed between a carbon center (C) and the radical species (X). It has been shown that the initial energy of this excited state is equal to $^3/_4$ of the singlet−triplet transition energy.[15] This is 2−4 eV higher than the ground state for most radical−alkene reactions. As overlap develops, the energy of this surface evolves in a manner similar to a Morse potential, given as a function of the C−X distance (r) by

$$E_{cov}(r) = {}^3/_4\Delta E_{ST} - ({}^3/_4\Delta E_{ST} - \Delta H)e^{-2\lambda(r-r_0)} \tag{3}$$

where $^3/_4\Delta E_{ST}$ is the initial energy of this surface, the quantity ($^3/_4\Delta E_{ST} - \Delta H$) is the fully evolved energy, and λ is the Morse decaying parameter. While an explicit treatment of the singlet−triplet surface energy is included in subsequent calculations, the energy does not develop appreciably in the far field.

Ionic Excited States. The ionic states are formed by transferring an electron from one species to the other. Initially, these surfaces are higher in energy than the ground state by the difference of the ionization potential of one species and the electron affinity of the other, IP − EA. There are several possible ionic states for a given radical−alkene system. The first possible excited state is formed by transferring an electron from the highest occupied molecular orbital (HOMO) of the molecule to the singly occupied molecular orbital (SOMO) of the radical. The second possible excited state is formed by transferring an electron from the SOMO of the radical to the lowest unoccupied molecular orbital (LUMO) of the alkene. For most radical−alkene systems, the radical is the better electron acceptor and the first state is lower in energy than the second. In the far field, both surfaces drop dramatically in energy as the reactants approach due to Coulombic attraction.

$$E_{Ionic}(r) = IP - EA - e^2/r \tag{4}$$

where r is the distance between the centers of charge of the two reactants. Other terms to account for the specific charge distribution and polarizability of the ions can also be included.[8] While the initial energies of these surfaces are significantly higher (8−15 eV above the ground state) than the covalent surfaces (2−4 eV) for most radical−molecule reactions, they drop by as much as 6−7 eV in the far field, and are frequently lower than the covalent surface at the boundary condition of the curve crossing.

Delocalization. Having established a framework for modeling the energies of the three reactant excited states, we seek to localize the interaction of the ground state to a single, mixed state. The construction of this state from the individual excited states requires an understanding of the relative degree to which each state mixes with the ground state. This mixing may be quantitatively determined using perturbation theory as described by Fukui and Fujimoto,[16] Salem,[17] and Libit and Hoffmann.[18] In the first stage of the reaction, where coupling is weak, the total interaction energy between the excited states and the ground state is given by

$$D = \sum_i^{Ex.State} \frac{(H_{Gnd,Ex} - S_{Gnd,Ex}H_{Gnd,Gnd})^2}{H_{Ex,Ex} - H_{Gnd,Gnd}} \tag{5}$$

where $H_{Gnd,Ex}$ is the interaction energy between the ground and an excited state, $S_{Gnd,Ex}$ is the overlap between the ground and excited state, $H_{Gnd,Gnd}$ is the ground-state energy, and $H_{Ex,Ex}$ is the excited-state energy. Under conditions where $H_{Gnd,Ex}$ is small, the numerator of eq 5 is proportional to the square of the overlap term, $S_{Gnd,Ex}^2$. Thus, the interaction energy for a

single excited state is proportional to

$$D \propto \frac{S_{\mathrm{Gnd,Ex}}{}^2}{H_{\mathrm{Ex,Ex}} - H_{\mathrm{Gnd,Gnd}}} \tag{6}$$

where the denominator represents the energy difference between the ground and excited states and is determined using either eq 3 or 4. The mixing of an excited state with the ground state describes the delocalization of electron density.

Multiple Excited States. At this point, we can construct a mixed reactant excited state to use in determining the two-state curve crossing height. To begin, we note that the adiabatic wave function of the interacting system in the absence of significant coupling is described by a linear combination of the ground- and excited-state wave functions, i.e.

$$\Psi_{\mathrm{ad}} = \frac{1}{\sqrt{a+b+c+d}}\{\sqrt{a}\Psi_{\mathrm{Gnd}} + \sqrt{b}\Psi_{(^3\mathrm{alk}^2\mathrm{X})} + \sqrt{c}\Psi_{(\mathrm{alk}^+\mathrm{X}^-)} + \sqrt{d}\Psi_{(\mathrm{alk}^-\mathrm{X}^+)}\} \tag{7}$$

At this stage in the reaction, the adiabatic wave function is similar to the unperturbed ground state; the coefficient, $\sqrt{a}$, of Ψ_{Gnd} is large. Consequently we may use a weak coupling approximation to assess the relative contributions of various excited states. The key assumption of this work is that we can construct a two-state crossing model based on this information.

The energy of this surface is given by

$$E_{\mathrm{ad}} = \frac{1}{a+b+c+d}\{aE_{\mathrm{Gnd}} + \underbrace{bE_{(^3\mathrm{alk}^2\mathrm{X})} + cE_{(\mathrm{alk}^+\mathrm{X}^-)} + dE_{(\mathrm{alk}^-\mathrm{X}^+)}}_{\text{excited state energies}} + E_{\mathrm{int}}\} \tag{8}$$

where the right-hand side is comprised of the weighted ground-state and excited-state energies followed by a term, E_{int}, describing the interaction energies among the various states, which is small. The ground-state energy and the excited-state energies are positive while the interaction energy is usually negative, reducing the energy of the system due to state mixing.

For the purposes of the two-state model, we seek a description of this system that yields the same result as eq 8 but reduced to only the ground state and a single (mixed) excited state, Ψ_{Mix}. This requires a total wave function composed solely of a ground and a mixed state, which is given by a linear combination of the singlet−triplet and both ionic states. The role of the ground-state wave function does not change in this simplified description, requiring that the normalization factor must be the same as in eq 7. Thus, this simplified wave function is

$$\Psi_{\mathrm{ad}} = \frac{\sqrt{a}\Psi_{\mathrm{Gnd}} + \sqrt{b+c+d}\Psi_{\mathrm{Mix}}}{\sqrt{a+b+c+d}} \tag{9}$$

and the energy is given by

$$E_{\mathrm{ad}} = \frac{1}{a+b+c+d}\{aE_{\mathrm{Gnd}} + \underbrace{(b+c+d)E_{\mathrm{Mix}}}_{\text{excited-state energy}} + E_{\mathrm{int}}{}'\} \tag{10}$$

As eqs 8 and 10 are equivalent, we now have an explicit solution for the mixed excited-state energy of

$$E_{\mathrm{Mix}} = \frac{1}{b+c+d}\{bE_{(^3\mathrm{alk}^2\mathrm{X})} + cE_{(\mathrm{alk}^+\mathrm{X}^-)} + dE_{(\mathrm{alk}^-\mathrm{X}^+)}\} \tag{11}$$

where coefficients b, c, and d are proportional to the relative delocalization energies. The mixed excited-state energy is therefore simply the average of the individual excited-state energies weighted by the interaction of each state with the ground state.

Finally, the mixed excited-state energy of the reactants can be calculated. Simplifying eq 11 with respect to the individual overlaps and energies, which comprise the delocalization energy of each reactant excited state, yields a mixed excited-state energy of

$$E_{\mathrm{Mix}} = \frac{S_{(^3\mathrm{alk}^2\mathrm{X})}{}^2 + S_{(\mathrm{alk}^+\mathrm{X}^-)}{}^2 + S_{(\mathrm{alk}^-\mathrm{X}^+)}{}^2}{(S^2/E)_{(^3\mathrm{alk}^2\mathrm{X})} + (S^2/E)_{(\mathrm{alk}^+\mathrm{X}^-)} + (S^2/E)_{(\mathrm{alk}^-\mathrm{X}^+)}} \tag{12}$$

The numerator is the sum of the squares of overlap between each excited state and the ground state, while the denominator is the total delocalization, D_{total}, which includes the sum of the contributions from the individual excited states.

We now make the approximation that this state is a boundary condition for a linear curve crossing, representing the nuclear and electronic distortions leading to the transition state (and ultimately to reaction products). Furthermore, we assume that the delocalization calculation (eq 6) is proportional to the coupling at the avoided curve crossing. Thus, we can construct a two-state model of barrier height evolution utilizing this mixed state.

Assuming that a two-state linear curve crossing correctly represents the ensuing reaction is no less accurate than the general application of a two-state model. In fact, it is more accurate. The crucial point is that we have localized the interaction of the ground state with the manifold of excited states on a single, mixed, excited state. This is mathematically equivalent to constructing a hybrid orbital. All of the interaction with the ground state is is confined to this single excited state (at the boundary), so any emerging interaction of other excited states with the ground state is strictly second order; the excited states may interact with each other, but this only influences the ground state through the resulting (second-order) perturbation. As we are focused on the adiabatic ground state, this is as it should be. Furthermore, we are interested primarily in the evolution of barrier heights from reaction to reaction. In the ensuing analysis, the influence of these second-order effects on barrier height evolution will be manifest as deviations of (perfect) data from the modeled evolution. Thus, only application to data will validate or refute our assumptions.

Choosing a Series of Reactions

In order to test the two-state model on reactive systems where multiple excited states may be important, we have chosen to examine the addition of H atoms to a series of alkenes and haloalkenes. This series provides a wide range of chemical properties, which affect both the energy (i.e., ionization potential, singlet−triplet splitting, etc.) and the spatial extent (i.e., π-electron density) of the three identifiable excited states interacting with the unperturbed ground state.

The appeal of H atoms is the lack of electrostatic perturbations in the far field as the reaction progresses. As the H atom approaches the alkene, there is no appreciable energetic well prior to the transition state from dipole interactions or p-orbital mixing. This is in contrast to hydroxyl radical or halogen atom addition reactions to alkenes,[19−21] in which a well prior to the transition state results in a complex potential energy surface and a negative temperature dependence. The ground-state energy

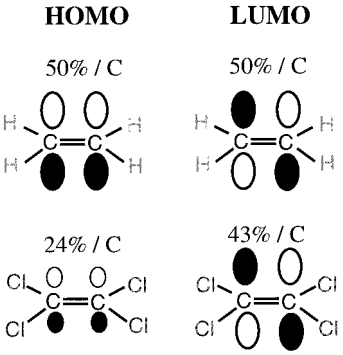

Figure 3. Graphical representation of the π system for the HOMO and LUMO of ethene and tetrachlorethene. The amount of electron density on each carbon is determined from ab initio calculations (UHF/6-31G**). There is much less electron density on the π carbons in the HOMO of tetrachloroethene. In the early stages of the reaction, there will be less interaction as a hydrogen approaches this species in comparison to ethene. The situation is similar although less severe for the LUMO.

for these H-atom reactions will be small and will not vary from reaction to reaction; thus we may ignore it in the curve crossing problem.

The appeal of the alkene/haloalkene series is that several molecular properties vary widely. While ionization potential and singlet−triplet splitting determine the energies of the individual excited states for the reaction with H, the presence of multiple excited states dictates the importance of the delocalization and, hence, overlap from one reaction to another. In particular, the electron density of the π bonds on the reactive carbons varies dramatically. This partially determines the overlap between the ground and excited states. As an example, the HOMO and LUMO of ethene and tetrachloroethene are illustrated in Figure 3. The electron density on a carbon in the HOMO of ethene is more than twice that of a carbon of tetrachloroethene. As the hydrogen atom begins to interact with these orbitals, there is significantly less overlap in the tetrachloroethene system. This difference is ultimately reflected in the delocalization. The overlap will be only somewhat more pronounced for the LUMO of tetrachloroethene.

Thus, we demand an ample dynamic range in H + alkene barrier heights to test this two-state model. This requirement necessitates the measurement of the temperature-dependent rate constants for a wide variety of reactions and indicates the need for a robust experimental technique. We must measure rate constants rapidly, with high precision and accuracy. In addition, we must cover a significant pressure and temperature range in order to guarantee that we are at the high-pressure limit for these addition reactions and to accurately measure the activation energy.

A large set of H-atom + alkene and haloalkene reactions is chosen to provide the dynamic range in reactivity. In particular, we will consider the following alkenes and haloalkenes: ethene, propene, isobutene, 2-ethyl-1-butene, *cis*-2-butene, *trans*-2-butene, and 2,3-dimethyl-2-butene, cyclopentene, cyclohexene, *cis*/*trans*-3,4-dimethyl-3-hexene, *trans*-1,2-dichloroethene, *cis*/*trans*-1,2-dibromoethene, and tetrachloroethene. For most compounds, both π carbons are equivalent and there is only one possible addition pathway.

Experimental Section

We use a high-pressure discharge-flow system (HPFS) with multiple H-atom resonance fluorescence (RF) axes to measure rate constants for these reactions. The instrument is shown in Figure 4, and essential components are labeled. The HPFS is strictly wall-less, with core-flow radical measurement, slow diffusion, and no movable injector. The core flow condition permits operation at essentially any pressure or temperature, and the multiple RF axes combined with computer control permit rapid measurements of rate constants. The technique has been extensively described,[9,22,23] and the experiment and data used in this work are discussed in detail in a companion paper.[24]

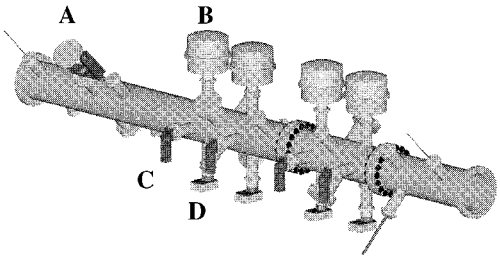

Figure 4. The high pressure flow system (HPFS) used for measuring the rate constants of atom−molecule reactions: (A) microwave plasma for the generation of hydrogen atoms, four resonance fluorescence axes comprised of (B) a lamp housing for the generation of Lyman-α light, (C) a photomultiplier tube for the detection of hydrogen fluorescence, and (D) a photodiode for the measurement of lamp flux.

TABLE 1: Activation Energies for Each Reaction

alkene	E_a, K
ethene[a]	993.9 ± 8.8
propene	812.6 ± 18.5
isobutene	457.1 ± 26.9
2-ethyl-1-butene	438.1 ± 28.3
cis-2-butene	1044.5 ± 20.4
trans-2-butene	1148.3 ± 26.5
2,3-dimethyl-2-butene	737.2 ± 7.2
cyclopentene	884.4 ± 12.6
cyclohexene	980.9 ± 23.5
3,4-dimethyl-3-hexene	936.4 ± 8.0
trans-1,2-dichloroethene	1372.9 ± 43.1
1,2-dibromoethene	1548.9 ± 39.6
tetrachloroethene	1736.0 ± 32.4

[a] From the literature.[25−27]

Hydrogen atoms are generated in a quartz sidearm using a microwave-induced plasma (A) and injected into the core of the N_2 carrier gas flow. Downstream, hydrogen atoms are detected with four RF axes at various locations along the flow tube. Each axis is comprised of a lamp (B) to generate Lyman-α light, a photomultiplier tube (C) to monitor hydrogen fluorescence, and a photodiode (D) to monitor lamp flux. Optical baffles restrict the atom detection to the central 8 cm^3 of the tube, yet permit sampling of sufficiently large solid angle to keep sensitivity high. The use of multiple detection axes allows radical decays to be monitored in real time without the temporal drifts associated with a single detection axis and a movable injector. This configuration is stable and precise; a rate constant can be measured in the span of 5−10 min.

All reactions were studied at 50 Torr total pressure from 298 to 370 K. At this pressure, most reactions were at or near their high-pressure limits. The rate constants correspond to the passage of reactants over the addition barrier, and a temperature dependence determines the barrier height. Only our measurements of H + ethene were not at the high-pressure limit; however, temperature-dependent data for this reaction are well constrained at high pressures.[25−27]

Measured activation energies for the reaction set are shown in Table 1. In each case, we assume that the reaction proceeds by a single pathway. While propene, isobutene, and 2-ethyl-1-butene have multiple pathways, radical attack is strongly favored

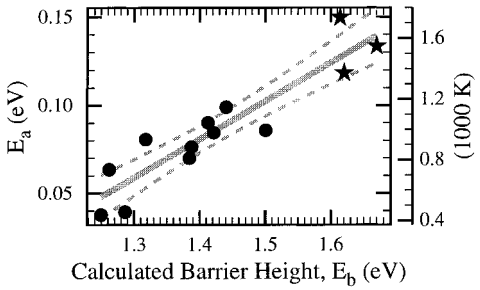

Figure 5. Measured activation energy, E_a, versus calculated barrier height, E_b. Haloalkene reactions are denoted by stars. The relationship is tight: the activation energy decreases as the calculated barrier height decreases. The solid gray line is a linear least-squares fit to the data, while the dashed lines show the (2σ) confidence interval of this result.

at the less-substituted π carbon (see Harris and Pitts[28] and references therein; verified by UHF/6-31G** calculations).

Results

The key test of the predictive capability of the two-state curve crossing model is the comparison of calculated barrier height to measured activation energy. The barrier height can be calculated using eqs 1 and 2, which require the enthalpy of reaction (ΔH), the energies of the reactant and product excited states (ΔE_R and ΔE_P), and the extent of coupling between the states when they are strongly mixed (β). The determination and use of these terms are presented in the Appendix. A comparison of calculated and measured barriers is shown in Figure 5. There is an excellent correlation (shown by the gray line) with a slope of 0.22 ± 0.03, verifying our ability to predict the evolution in barrier height for radical−molecule addition reactions. For this set of reactions, no other model that we have explored, including a singlet−triplet splitting model and empirical models based on reaction enthalpy or IP − EA, can successfully predict this evolution in E_b. The linear relationship between measured activation energy and calculated barrier height holds over the full range of reactions, which spans more than a factor of 4 in measured activation energy. However, the calculated barrier height is substantially larger than the measured activation energy. Three factors contribute to this: we have certainly underestimated the coupling, we have assumed a linear evolution in diabatic state energies, which is certainly not quantitatively correct, and we have neglected tunneling, which lowers the activation energy with respect to the barrier height.

Evaluation of Terms. We can now quantitatively assess the role of specific parameters in controlling the observed barrier heights. To do this, we examine the derivative of E_b in eq 2 with respect to each term contributing to barrier height. We plot these derivatives against the measured barrier height for each reaction in the series. A controlling parameter will show a tight, positive correlation that spans a substantial portion of the observed range. In this context, the total derivative for a series of reactions (rxn) is given by

$$\frac{dE_b}{d(rxn)} = \frac{\partial E_b}{\partial(\Delta H)}\frac{d(\Delta H)}{d(rxn)} + \frac{\partial E_b}{\partial(\Delta E_P)}\frac{d(\Delta E_P)}{d(rxn)} + \frac{\partial E_b}{\partial(\Delta E_R)}\frac{d(\Delta E_R)}{d(rxn)} + \frac{\partial E_b}{6\beta}\frac{d\beta}{d(rxn)} \quad (13)$$

The derivative of E_b with respect to each term is multiplied by the variability of that term over the series of reactions. The variability is taken to be the deviation from the average, for example

$$\frac{d(\Delta H)}{d(rxn)} = (\Delta H_i - \langle \Delta H \rangle) \quad (14)$$

where ΔH_i is the enthalpy for a particular reaction and $\langle \Delta H \rangle$ is the expectation value for the series. This places the average magnitude of variation in barrier height at zero. The explicit derivative with respect to each term is then easily determined. These derivatives (with respect to reaction enthalpy, reactant and product excited-state energies, and reaction coupling) are given by

$$\frac{\partial E_b}{\partial(\Delta H)}\frac{d(\Delta H)}{d(rxn)} = \frac{E_R(1-\beta)}{E_R + E_P}(\Delta H_i - \langle \Delta H \rangle) \quad (15)$$

$$\frac{\partial E_b}{\partial(\Delta E_R)}\frac{d(\Delta E_R)}{d(rxn)} = \frac{E_P(\Delta H + E_P)(1-\beta)}{(E_R + E_P)^2}(\Delta H_i - \langle \Delta H \rangle)(\Delta E_{R,i} - \langle \Delta ER \rangle) \quad (16)$$

$$\frac{\partial E_b}{\partial(\Delta E_P)}\frac{d(\Delta E_P)}{d(rxn)} = \frac{E_R(\Delta H - E_R)(1-\beta)}{(E_R + E_P)^2}(\Delta E_{P,i} - \langle \Delta E_P \rangle) \quad (17)$$

$$\frac{\partial E_b}{\partial(\Delta E_P)}\frac{d\beta}{d(rxn)} = -\frac{E_R(\Delta H + E_P)}{E_R + E_P}(\beta_i - \langle \beta \rangle) \quad (18)$$

Results are shown in Figure 6 and discussed below. The full range of variation in the derivatives is used for all plots to allow a comparison of the role of each term. In addition, the trend from Figure 5 is shown in each derivative plot. A positive correlation between an individual term and measured barrier height is indicated by a positive slope.

It is evident from Figure 6 that neither the reaction enthalpy (ΔH) nor the coupling (β, related to the delocalization, D) contribute significantly to the evolution in barrier height. Qualitatively from eq 2, the barrier height should decrease as the reaction becomes more exothermic. From Figure 6a, it is seen that enthalpy does not contribute in this way to the observed trend in barrier height versus measured activation energy. If anything, there is a negative correlation; this derivative opposes the variation in barrier height for the higher barrier reactions (H + halogenated alkenes). The enthalpy of reaction, therefore, is not driving reactivity in the H + alkene series.

The coupling between the ground and excited states is related to the total delocalization of the individual reactant excited states as discussed above. A relationship between activation energy and delocalization is observed (see Appendix); barrier height decreases as delocalization increases in magnitude. Using the total delocalization as a surrogate for coupling, the derivative of barrier height with respect to coupling can be evaluated. For the series, the delocalization does contribute in a positive sense to the trend (gray line) in activation energy versus barrier height, as shown in Figure 6b. However, this contribution is small. This is not to say that changes in coupling do not in general change barrier height—they obviously do—but rather that, in this series, this effect is secondary.

Taken together, the reactant and product excited states dominate the evolution of reactivity in this series. From eq 1, the barrier to reaction decreases as the reactant and product energy gaps decrease. The specific contributions of these terms to the trend in barrier height are shown in Figure 6c,d.

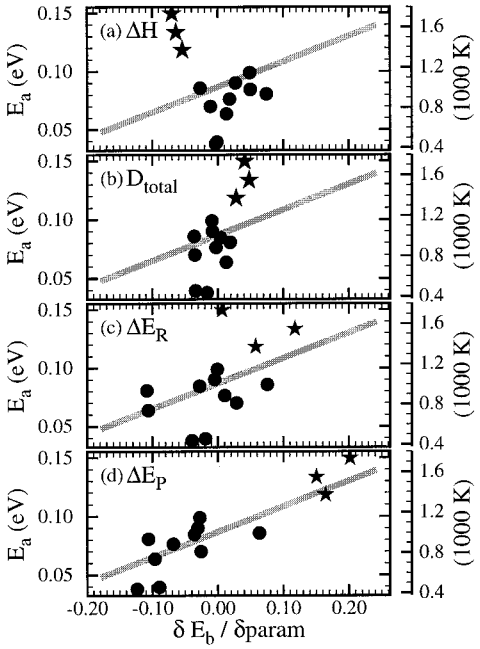

Figure 6. Derivative of the barrier height with respect to (a) enthalpy, (b) total delocalization, (c) reactant energy gap, and (d) product energy gap. Haloalkene reactions are denoted by stars. The driving forces for the reactivity of hydrogen atoms with alkenes are the reactant (mixed) and product excited-state energies. The gray lines show the trend from Figure 5.

Both the reactant and product excited states are mixed (at least conceptually). However, we have only explicitly treated this mixing for the reactants. We can now use the same derivative approach to evaluate the influence of the component excited-state energies on this mixed energy. Taking the derivative of this energy with respect to an individual excited-state energy, E_j, yields

$$\frac{\partial(E_{\mathrm{Mix}})}{\partial(\Delta E_j)} = \frac{D_j(E_{\mathrm{Mix}}/E_j)}{D_{\mathrm{total}}}(\Delta E_{j,i} - \langle \Delta E_j \rangle) \qquad (19)$$

where E_{Mix} is the mixed excited-state energy, E_j is the energy of an individual surface, D_{total} is the total delocalization (from eq 5), and D_j is the delocalization from an individual surface. The results for each initial reactant energy are shown in Figure 7.

Neither the higher ionic state (Figure 7a) nor the singlet−triplet state (Figure 7b) influences E_{Mix} in a manner consistent with the observed barrier height evolution. In both cases, there is negligible variation for the alkenes and an influence opposite that observed for the haloalkenes; the activation energy is high despite a downward trend by both states. The lower ionic surface, on the other hand, does show a controlling influence (Figure 7c).

The large derivative in Figure 7c indicates that the ionic surface significantly influences the energy of the mixed excited state, and the general positive trend shows the influence to be consistent with the observed barriers. Within the overall relationship two trends stand out: four lower barrier reactions form one trend, while the higher barrier reactions constitute another. Each of the molecules (2-ethyl-1-butene, isobutene, propene, and ethene) of the lower trend has at least one unsubstituted π carbon. These reactions have higher energies at the boundary condition to the curve crossing. However, this energetic influence is offset by greater overlap with the attacking

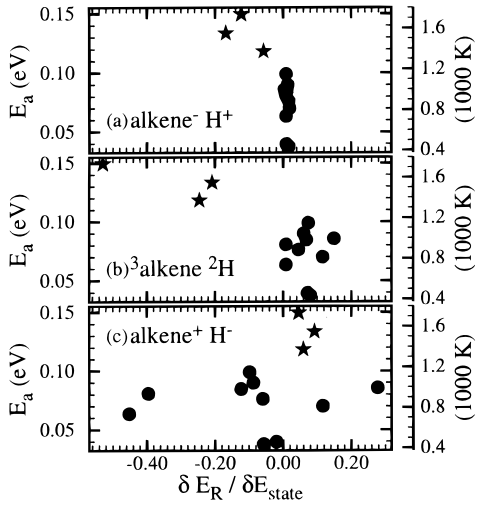

Figure 7. Derivative of the mixed excited-state energy with respect to (a) the (alkene$^-$H$^+$) energy, (b) the (^{3}alkene^{2}H) energy, and (c) the (alkene$^+$H$^-$) energy. Haloalkene reactions are denoted by stars. For the nonhalogenated alkene reactions, the singlet−triplet and higher ionic surface energies are nearly invariant.

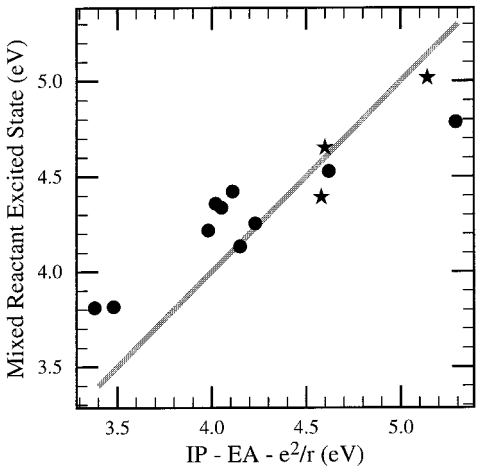

Figure 8. Mixed excited-state energy of the reactants versus the height of the ionic surface at the end of the reactant approach stage. The 1:1 line is shown in gray. The ionic energy governs the mixed excited-state energy, although the other excited states continue to play a small role.

radical than all other alkenes, resulting in larger delocalizations than in reactions of the other trend.

To further investigate the role of the ionic state, we plot the height of the ionic surface at the boundary condition to the curve crossing versus the mixed excited-state energy (shown in Figure 8). This plot does not depend on experimental rate measurements, but is the result of the simple calculations discussed above. A tight relationship is observed. The mixed excited-state energy of the reactants is proportional to the height of the ionic surface. However, the slope is less than 1 (the 1:1 line is shown in gray), indicating that the other excited states do contribute to a small extent.

Discussion

The evolution in barrier height for the reactions of H with several alkenes and haloalkenes is determined largely by the energies of the reactant and product excited states at the boundary condition to the curve crossing. The energy of the reactant excited state is determined from a manifold of excited states, with variability driven primarily by the lowest ionic

surface (alkene$^+$H$^-$). However, accurate predictive capability is only achieved by incorporating many facets of the reactive system into the modified two-state model, such as reaction enthalpy and the covalent excited state energy, in addition to the states mentioned above. By including multiple states, it is possible to smoothly model the transition from reactions controlled by ionic states to reactions controlled by covalent (singlet−triplet) states, while correctly identifying the dominant state in each case.

For example, in a study of the addition of CH_3 to various substituted alkenes,[10,11] it was determined that the barrier height was governed by a crossing between the ground and the singlet−triplet states of the reactants. This triplet surface maps into the ground state of the products, leading to a correlation between barrier height and reaction enthalpy. In those studies, it was concluded that ionic states are not influencing the barrier height due to the lack of charge transfer or polarity at the transition state. While charge separation at the transition state necessitates the involvement of ionic excited states, a lack of polarity does not preclude the participation of multiple ionic states in which the charges cancel. Nevertheless, this conclusion is reasonable for methyl radical additions. The energies of the ionic surfaces in the addition of CH_3 to an alkene are substantially higher than the covalent surface. This is due to the negative electron affinities of CH_3 and the alkenes, resulting in high excited-state energies, and, hence, low delocalizations for the (alkene$^+$$CH_3^-$) and (alkene$^-$$CH_3^+$) surfaces, respectively; the barrier is largely the result of the crossing between the ground state and the covalent excited state.

In contrast, the reactivity of hydroxyl radicals with alkenes was analyzed by Abbatt et al.,[19] who observed a strong correlation between room-temperature rate constant and alkene ionization potential. The electron affinity of the hydroxyl radical is quite large (EA = 1.83 eV),[29] significantly lowering the initial energy of the (alkene$^+$OH$^-$) surface relative to other surfaces, and increasing its coupling with the ground state. In these reactions, the barrier to addition is defined largely by the crossing of the ground and lowest ionic states. A similar result was obtained for the hydrogen atom abstraction reactions of various radicals with alkanes.[8,9]

Here we have a middle ground; in the reactions of H with alkenes and haloalkenes, the singlet−triplet surface contributes most strongly to the individual barriers, but this contribution is nearly constant over the full range of reactions. Variability of the reactant excited state is, in fact, driven by the lowest ionic surface (see Figure 7c). The energy of this surface is intermediate to the ionic states of the CH_3 and OH reactions, and overlap varies widely. In calculating a mixed excited state to use as a boundary condition for the two-state crossing, the contribution of the ionic surfaces is quantitatively weighed against the contribution of the covalent surface. Over the series of reactions, the lowest ionic surface dominates the evolution of the mixed excited-state energy and, therefore, barrier height.

These conclusions will apply to electrophilic radicals. For example, we again consider OH addition reactions. As mentioned above, Abbatt et al.[19] observed a strong correlation between ionic energy and k_{298} for OH + alkene reactions. However, this correlation did not extend to haloalkenes. We can now describe qualitatively what drives these observations, and we expect further work to support a quantitative analysis. Two factors discussed in this work complicate the OH−alkene system: a large, evolving ground-state energy, and significant changes in π-electron density. These OH addition reactions are characterized by a dipole−induced dipole well prior to the addition transition state, which lowers the energy of the system below reactants. Due to this well, negative temperature dependences are measured for these reactions, hindering direct determination of the addition barrier heights. We expect, however, that the processes governing barrier height in OH-addition reactions will mirror those observed here for H-addition reactions. Ionic-state energies will exhibit the same trends, but will have significantly lower initial energies (the EA of OH is 1 eV greater than that of H[29]), so the mixed state will be more strongly dominated by ionic states. The observed relationship between k_{298} and IP − EA for the OH−alkene reactions is thus expected. However, just as overlap, driven by π-electron density, weakens the coupling for H−haloalkene reactions and raises the barrier height, the reduced overlap of the OH−haloalkene series raises barrier height with respect to their unsubstituted analogues. At the extreme, the barrier for OH + tetrachloroethene is above the reactant energy, unlike virtually all other OH−alkene and OH−haloalkene reactions.

Conclusions

In this study, the two-state crossing model has been expanded to explicitly treat systems with multiple reactant excited states. Mixed states were constructed from the weighted averages of the individual excited states and used as boundary conditions to the linear crossing. The energies of these mixed states, along with the energies of the product excited states, reaction enthalpies, and total delocalizations of the individual reactant states, were used to calculate barrier heights. The predictive capability of this model was confirmed by examining H-atom addition reactions to alkenes; the activation energy decreases as the calculated barrier height decreases. Moreover, the role of each individual property of the system in determining barrier height was determined through the derivative of barrier height with respect to that property. The driving forces for the reactivity of these systems are the reactant and product excited-state energies. Within this approach, a closer examination of the nature of the mixed reactant excited state reveals it to be similar to the ionic state formed by transferring electron density from the alkene to the hydrogen atom.

Acknowledgment. This work was supported by NSF Grant 9414843 to Harvard University.

Appendix: Crossing Height Parameters

The calculation of barrier height from eqs 1 and 2 requires the reaction enthalpy, the reactant and product excited-state energies, and an understanding of the coupling between the ground and excited states (i.e., β). In this section, the determination and use of each of these terms is described. All data used in these calculations are presented in Table 2.

Reaction Enthalpy. Reaction enthalpies are determined using ab initio calculations (UHF/6-31G**, UHF/6-311G** for 1,2-dibromoethene) corrected for zero-point energy differences. While there are little experimental data for these systems, the calculated enthalpies for the reactions of H + ethene, propene, and *cis*-2-butene are found to be in good agreement with experiment.[29−32] All reactions are highly exothermic, with enthalpies ranging from −1.40 eV (32.3 kcal) for H + 3,4-dimethyl-3-hexene to −1.74 eV (40.1 kcal) for H + tetrachloroethene. In general, the reactions of H atoms with halogen-substituted alkenes exhibit the largest enthalpies, while reactions of H atoms with hydrocarbon substituents on the carbons of the π system exhibit the lowest enthalpies.

TABLE 2: Values Used in Calculating the Evolved Excited State Energies, Delocalizations, and the Two-State Crossing Height

compound	ST[c]	evol	IP[d]	evol	EA[e]	evol	prod[f]	ΔH[g]	O_{HO}	O_{LU}[h]
ethene	3.23	−0.36	10.51	−4.52	−2.63	−4.91	5.05	−1.63	0.498	0.495
propene	3.21	−0.37	9.73	−4.41	−2.77	−4.71	4.74	−1.56	0.502	0.469
isobutene	3.17	−0.37	9.22	−4.29	−2.79	−4.87	4.52	−1.57	0.513	0.431
2-ethyl-1-butene	3.17	−0.35	9.06	−4.21	−2.63	−4.38	4.41	−1.58	0.503	0.365
cis-2-butene	3.16	−0.38	9.11	−4.36	−2.89	−4.96	4.72	−1.51	0.429	0.433
trans-2-butene	3.18	−0.38	9.10	−4.38	−2.88	−5.04	4.73	−1.46	0.426	0.440
cyclopentene	3.14	−0.38	9.01	−4.27	−2.83	−4.86	4.60	−1.53	0.407	0.444
cyclohexene	3.18	−0.38	8.95	−4.27	−2.81	−4.88	4.70	−1.46	0.423	0.383
2,3-dimethyl-2-butene	3.08	−0.36	8.27	−4.19	−2.84	−4.88	4.48	−1.54	0.397	0.330
3,4-dimethyl-3-hexene	3.08	−0.36	8.17	−3.99	−2.74	−4.78	4.44	−1.40	0.394	0.312
trans-1,2-dichloroethene	2.88	−0.39	9.64	−4.34	−2.00	−4.95	5.43	−1.70	0.282	0.468
1,2-dibromoethene	2.94	−0.41	9.55	−3.71	−1.81	−5.32	5.33	−1.71	0.208	0.475
tetrachloroethene	2.65	−0.39	9.33	−4.05	−1.61	−5.19	5.62	−1.74	0.243	0.432

[a] EA(H) = 0.7 eV.[33] [b] IP(H) = 13.59 eV.[33] [c] Initial energy of the singlet−triplet surface (eV). The values for 2-ethyl-1-butene, 3,4-dimethyl-3-hexene, and 1,2-dibromoethene are estimated (see text). The evolution of this surface is calculated using a Morse stretching parameter of $\lambda = 1.95$.[34] [d] Ionization potential of the alkenes (eV). The evolution of the corresponding surface up to the boundary condition is also given. [e] Electron affinities of the alkenes (eV). The evolution of the corresponding surface is also given. [f] Product excited-state energy (eV). [g] Reaction enthalpy (eV). [h] Occupancies of the HOMO and LUMO of the reactive carbons of the alkenes.

Reactant (Mixed) Excited State. The determination of the mixed excited-state energy from eq 12 requires both the energies of the component excited states and the overlaps of these states with the ground state. This mixed energy can then be used as a boundary condition to the two-state curve crossing.

To determine the energies of each reactant excited state, the transition-state structure for each reaction studied is calculated using UHF/6-31G**, giving an invariant carbon−hydrogen bond length of close to 2 Å. These calculations further indicate that the rehybridization of the reactive carbon (from $sp^2 \rightarrow sp^3$) begins when the attacking hydrogen atom is approximately 0.75 Å further away from the reactive carbon than at the transition state. Given that this rehybridization is induced by the significant onset of overlap, this distance (∼2.75 Å) is used to mark the end of the reactant approach stage. With this distance as a boundary condition to the crossing, the evolution of the reactant excited states can be modeled according to the methods described above. Literature values for the experimentally determined singlet → triplet excitation energies and ionization potentials are used when available.[33,35,36] Because experimental singlet−triplet energies are available for only a few product radicals, we use those values to calibrate ab initio calculations (UHF/6-31G**) of vertical singlet−triplet energies for the entire reaction set. Electron affinities of the alkenes are also determined using ab initio calculations (UHF/6-31G**). A Morse decaying parameter of 1.95 $Å^{-1}$ is used in modeling the evolution of the singlet → triplet surface,[34] while simple Coulombic attraction governs the evolution of the ionic excited states.

The coupling of each excited state to the ground state is assessed by calculating the delocalization energy as described earlier, which is partially determined by overlap between the states. The boundary conditions imposed by this model, however, rely on the absence of strong state mixing or overlap. Therefore, we calculate the propensity for delocalization of each excited state in its interaction with the ground state.

To calculate the propensity for delocalization, we assume that overlap between the ground state and an excited state is principally governed by the overlap between the frontier orbitals on the reactive sites. For the case of single-site attack, the overlap can be expressed as

$$S_{SOMO,MO} = c_1 \phi_s \phi_p \tag{20}$$

where ϕ_s is the hydrogen s orbital, ϕ_p is the atomic orbital on the reaction carbon of the alkene, and c_1 is the coefficient of ϕ_p in the relevant molecular orbital.

Ab initio calculations using the Hartree−Fock level of theory indicate that the transition-state geometries for these reactions are similar. While this is a first-order approximation (higher level calculations show slightly varying geometries), the geometric overlap between the reactive atomic orbitals is assumed to develop similarly from reaction to reaction. Thus, the overlap between the ground and excited states varies from reaction to reaction with the coefficient on the p orbital of the reacting carbon, c_1. In a larger basis-set representation, in which not all of the electron density is on a single p orbital of the reacting carbon in a particular molecular orbital, the overlap is related to the number of electrons localized on the reactive carbon within the reactive MO. This is the orbital occupancy of the carbon and is given by

$$O_{MO}^{atom} = \sum_{i}^{atom} \sum_{j}^{MO} c_i c_j \phi_i \phi_j \tag{21}$$

where i represents the atomic orbitals on the reacting carbon in the MO of interest and j represents all of the atomic orbitals in that MO. In this regard, a value that accurately indicates the role of each excited state can be determined in the absence of a large degree of overlap. We can now express the overlap of interacting excited states by

$$S_{(^3\text{alkene}^2\text{H})} \propto (O_{HO} + O_{LU})^2 \tag{22}$$

$$S_{(\text{alkene}^+\text{H}^-)} \propto (2O_{HO})^2 \tag{23}$$

$$S_{(\text{alkene}^-\text{H}^+)} \propto (2O_{LU})^2 \tag{24}$$

where O_{HO} and O_{LU} are the electron densities (normalized to the number of electrons) on a p carbon in the HOMO and LUMO of the alkene, respectively.

Propensity for delocalization of each excited state has been calculated for each reaction studied here using eqs 3, 4, and 6, allowing the mixed excited-state energies to be determined. The results of these delocalization calculations are plotted against activation energy and shown graphically in Figure 9. The ranges of these plots are fixed to the full range of the data to indicate both relative magnitude and variability. Results are discussed below.

The initial energies of the singlet−triplet surface are low in comparison to the other excited states (see Table 2). The subsequent evolution in energy from the initial splittings,

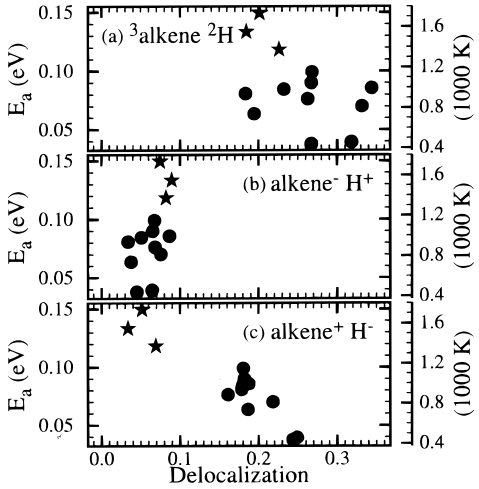

Figure 9. Measured activation energy versus the propensity for delocalization. (a) The plot for the singlet−triplet surface (^{3}alkene^{2}H) shows large but scattered degrees of delocalization. (b) The highest ionic surface (alkene$^-$H$^+$) is essentially constant, with a low magnitude. (c) The lowest ionic surface (alkene$^+$H$^-$) varies by a factor of 5 and shows a tight correlation. These values, once normalized, determine the coefficients for the mixed excited-state energy of the reactants.

however, is small for these surfaces (∼0.4 eV). This indicates that overlap is small at this point along the reaction and further validates the choice of boundary conditions for the two-state crossing. The occupancy of this surface is large, but changes only slightly from reaction to reaction, governed primarily by the changing π structure of the HOMOs. Together, the low energy and large overlap result in a large degree of delocalization relative to the other excited states. While a trend in Figure 9a can be argued, it is minimal with large scatter.

The delocalization resulting from the higher ionic surface is shown in Figure 9b. For all reactions studied here delocalization is small and constant in comparison to the other terms. The occupancies of the LUMOs are less variable than those of the HOMOs. In addition, the surfaces are much higher in energy than the other surfaces at this stage of the reaction, despite the large Coulombic attraction between the ions. Thus, this surface is relatively unimportant in determining the energy of the mixed excited state.

The delocalization resulting from the lower ionic surface is smaller than that from the singlet−triplet surface as shown in Figure 9c. It is, however, highly variable and shows a tight correlation with activation energy. Unlike the energies of the singlet−triplet surfaces, the energies of the ionic surfaces have dropped dramatically (∼4 eV) from their initial values at this point along the reaction. Lower barrier reactions have as much as 5 times more delocalization than higher barrier reactions. The range in delocalization arises from variability in both excited-state energy and overlap. For example, tetrachloroethene has one of the highest ionic surface energies for a substituted alkene. In addition, chlorine atoms withdraw electron density from the carbon−carbon π bond, thereby reducing the electron density on the carbons available for the formation of a bond. This results in less delocalization from this excited state than from excited states of other reactants.

Product Excited States. It is difficult to determine the appropriate excited state of the products to use as a boundary condition for the two-state model in a manner consistent with the boundary conditions used for the reactants. This difficulty arises because the product is a single molecule; as such, excited states (analogous to the reactants) created by transferring electron density from one separated species to another cannot be identified. The excited states of the product alkyl radical are already strongly mixed, preventing them from being correlated to intramolecular (bond) triplets or zwitterions. The approach taken here is, therefore, to use the first spectroscopic excited state of the alkyl radical as a indicator of the mixed excited-state energy.

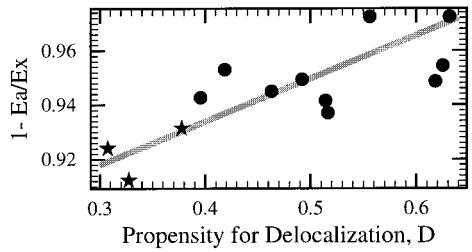

Figure 10. The quantity $(1 - E_a/E_X)$ vs total delocalization, showing the relationship between the coupling constant, β, and the total delocalization of the reactants. The intercept is large, indicating a strong coupling between the ground and excited states. The slope indicates a positive but small dependence; the coupling increases with increasing delocalization.

The energies for the first excited state of a few alkyl products have been previously measured by modulated UV-absorption spectrometry.[37] These energies have been shown to correlate with the first ionization potential of the alkyl radical.[38] The measured excited-state energies and ionization potentials, however, are limited to a small subset of alkyl products for the reactions studied here. With the above correlation as a guideline, theoretically determined ionization potentials for all reaction products (UHF/6-31G**) are used to establish the excited-state energies. While these ionization potentials are substantially lower than the experimentally determined values for the available compounds,[33] they provide a consistent approximation to the product excited-state energy. It is important to note, however, that these calculations represent a source of uncertainty within this study and indicate a need for further experimental studies of alkyl radical excited states.

β-Dependence. The reactions studied here are strongly coupled; the interaction between the unperturbed ground state and the excited state is large, splitting their energies and producing the adiabatic reaction surface. We assume that this energy splitting is related to the total delocalization, i.e.

$$\beta = FD_{\text{total}} \tag{25}$$

where β is a measure of the coupling between the ground and excited states, F is a proportionality constant, and D_{total} is the sum of the electron delocalizations from each excited state. The influence of the total delocalization of the reactants on barrier height from reaction to reaction can be tested through eq 2. If there is indeed a relationship between β and delocalization (i.e., if eq 25 is a reasonable assumption), then the quantity $(1 - E_a/E_X)$ should correlate with D_{total}. This is shown in Figure 10, and a clear correlation is observed. As the delocalization increases, E_a/E_X approaches zero. The fit to the data, however, reveals a small slope ($F = 0.155$) with a large intercept (0.871), indicating strong but relatively constant coupling. Possible reasons for this large intercept include the delocalization from the product excited state, which has been neglected (i.e., β should be proportional to delocalization from both the reactant and product excited states). In addition, the explicitly calculated delocalization energy may have a much larger slope over the series of reactions. Namely, the assumptions about delocalization are reasonable for understanding trends, but are oversimplified in accurately predicting magnitude.

References and Notes

(1) Giese, B.; *Angew. Chem., Int. Ed. Engl.* **1983**, *22*, 753.
(2) Carey, F. A.; Sundberg, R. J. *Advanced Organic Chemistry. Part A: Structure and Mechanisms*; Plenum Press: New York, 1990.
(3) Seinfeld, J. H. et al. *Rethinking the ozone problem in urban and regional air pollution*; Technical Report; National Research Council, 1992.
(4) Atkinson, R. *J. Phys. Chem. Ref. Data* **1997**, *36*, 75.
(5) Atkinson, R.; Aschmann, S. M.; Fitz, D. R.; Winer, A. M.; Pitts, J. N. *Int. J. Chem. Kinet.* **1982**, *14*, 13.
(6) Silver, D. M. *J. Am. Chem. Soc.* **1974**, *96*, 5959.
(7) Pross, A. *Theoretical and Physical Principles of Organic Reactivity*; John Wiley and Sons: New York, 1995.
(8) Donahue, N. M.; Clarke, J. S.; Anderson, J. G. *J. Phys. Chem.* **1998**, *102*, 3923.
(9) Clarke, J. S.; Kroll, J. H.; Donahue, N. M.; Anderson, J. G. *J. Phys. Chem.* **1998**, *102*, 9847.
(10) Wong, M. W.; Pross, A.; Radom, L. *J. Am. Chem. Soc.* **1993**, *115*, 11050.
(11) Wong, M. W.; Pross, A.; Radom, L. *J. Am. Chem. Soc.* **1994**, *116*, 6284.
(12) Truhlar, D. G.; Garrett, B. C.; Klippenstein, S. J. *J. Phys. Chem.* **1996**, *100*, 12771.
(13) Melissas, V. A.; Truhlar, D. G. *J. Chem. Phys.* **1993**, *99*, 1013.
(14) Shaik, S. S.; Hiberty, P. C. *Adv. Quantum Chem.* **1995**, *26*, 99.
(15) Shaik, S. S.; Hiberty, P. C.; Lefour, J. M.; Ohanessian, G. *J. Am. Chem. Soc.*, **1987**, *109*, 363.
(16) Fukui, K.; Fujimoto, H. *Bull. Chem. Soc. Jpn.* **1968**, *41*, 1989.
(17) Salem, L. *J. Am. Chem. Soc.* **1968**, *90*, 543.
(18) Libit, L.; Hoffmann, R. *J. Am. Chem. Soc.* **1974**, *96*, 1370.
(19) Abbatt, J. P. D.; Anderson, J. G. *J. Phys. Chem.* **1991**, *95*, 2382.
(20) Engels, B.; Peyerimhoff, S. D. *J. Phys. Chem.* **1989**, *93*, 4462.
(21) Engels, B.; Peyerimhoff, S. D.; Skell, P. S. *J. Phys. Chem.* **1989**, *94*, 1267.
(22) Abbatt, J. P. D.; Demerjian, K. L.; Anderson, J. G. *J. Phys. Chem.* **1990**, *94*, 4566.
(23) Donahue, N. M.; Clarke, J. S.; Demerjian, K. L.; Anderson, J. G. *J. Phys. Chem.* **1996**, *100*, 5821.
(24) Clarke, J. S.; Kroll, J. H.; Rypkema, H. A.; Donahue, N. M.; Anderson, J. G. *J. Phys. Chem.*, in press.
(25) Lee, J. H.; Michael, J. V.; Payne, W. A.; Stief, L. J. *J. Chem. Phys.* **1978**, *68*, 1817.
(26) Kyogoku, T.; Watanabe, T.; Tsunashima, S.; Sato, S. *Bull. Chem. Soc. Jpn.* **1981**, *54*, 2872.
(27) Lightfoot, P. D.; Pilling, M. J. *J. Phys. Chem.* **1987**, *91*, 3373.
(28) Harris, G. W.; Pitts, J. N. *J. Chem. Phys.* **1982**, *77*, 3994.
(29) Mallard, W. G. *NIST Chemical Kinetics Database*; Technical Report 17; NIST, 1994.
(30) Nicovich, J. M.; van Dijk, C. A.; Kreutter, K. D.; Wine, P. J. *J. Phys. Chem.* **1991**, *95*, 9890.
(31) Seakins, P. W.; Pilling, M. J.; Niiranen, J. T.; Gutman, D.; Krasnoperov, L. N. *J. Phys. Chem.* **1992**, *96*, 9847.
(32) Hanning-Lee, M. A.; Green, N. J. B.; Pilling, M. J.; Robertson, S. H. *J. Phys. Chem.* **1993**, *97*, 860.
(33) Mallard, W. G. *NIST chemistry Webbook*; Technical Report 69; NIST, 1997. http://webbook.nist.gov/.
(34) Pais, A. A. C. C.; Arnaut, L. G.; Formosinho, S. J. *J. Chem. Soc., Perkin Trans. 2* **1998**, 2577.
(35) Flicker, W. M.; Mosher, O. A.; Kuppermann, A. *Chem. Phys. Lett.* **1975**, *36*, 56.
(36) Koerting, C. F.; Walzl, K. N.; Kuppermann, A. *Chem. Phys. Lett.* **1984**, *109*, 140.
(37) Wendt, H. R.; Hunziker, H. E. *J. Chem. Phys.* **1984**, *82*, 717.
(38) Lengsfield, B. H.; Siegbahn, P. E. M.; Liu, B. *J. Chem. Phys.* **1984**, *81*, 710.